

3D UX-NET: A LARGE KERNEL VOLUMETRIC CONVNET MODERNIZING HIERARCHICAL TRANSFORMER FOR MEDICAL IMAGE SEGMENTATION

Ho Hin Lee *

Vanderbilt University

Shunxing Bao

Vanderbilt University

Yuankai Huo

Vanderbilt University

Bennett A. Landman

Vanderbilt University

ABSTRACT

Vision transformers (ViTs) have quickly superseded convolutional networks (ConvNets) as the current state-of-the-art (SOTA) models for medical image segmentation. Hierarchical transformers (e.g., Swin Transformers) reintroduced several ConvNet priors and further enhanced the practical viability of adapting volumetric segmentation in 3D medical datasets. The effectiveness of hybrid approaches is largely credited to the large receptive field for non-local self-attention and the large number of model parameters. We hypothesize that volumetric ConvNets can simulate the large receptive field behavior of these learning approaches with fewer model parameters using depth-wise convolution. In this work, we propose a lightweight volumetric ConvNet, termed 3D UX-Net, which adapts the hierarchical transformer using ConvNet modules for robust volumetric segmentation. Specifically, we revisit volumetric depth-wise convolutions with large kernel size (e.g. starting from $7 \times 7 \times 7$) to enable the larger global receptive fields, inspired by Swin Transformer. We further substitute the multi-layer perceptron (MLP) in Swin Transformer blocks with pointwise depth convolutions and enhance model performances with fewer normalization and activation layers, thus reducing the number of model parameters. 3D UX-Net competes favorably with current SOTA transformers (e.g. SwinUNETR) using three challenging public datasets on volumetric brain and abdominal imaging: 1) MICCAI Challenge 2021 FLARE, 2) MICCAI Challenge 2021 FeTA, and 3) MICCAI Challenge 2022 AMOS. 3D UX-Net consistently outperforms SwinUNETR with improvement from 0.929 to 0.938 Dice (FLARE2021) and 0.867 to 0.874 Dice (FeTA2021). We further evaluate the transfer learning capability of 3D UX-Net with AMOS2022 and demonstrates another improvement of 2.27% Dice (from 0.880 to 0.900). The source code with our proposed model are available at <https://github.com/MASILab/3DUX-Net>.

1 INTRODUCTION

Significant progress has been made recently with the introduction of vision transformers (ViTs) Dosovitskiy et al. (2020). ViTs consistently demonstrate superior performance over the convolutional networks (ConvNets) in both natural image and medical domain Chen et al. (2021a); Bhojanapalli et al. (2021); Yu et al. (2021); Wang et al. (2021b); Li et al. (2022b). Specifically, ViTs demonstrate their abilities in 3D to extract sequential representation with volumetric patches and generate non-local self-attentions correspondence to enhance volumetric-related downstream tasks, especially for medical image segmentation Wang et al. (2021a); Hatamizadeh et al. (2022b); Zhou et al. (2021). Another characteristic of ViTs is the lack of image-specific inductive bias and the scaling behaviour which are enhanced by large model capacities and dataset sizes. Both characteristics contribute to the significant improvement compared to ConvNets on medical image segmentation Tang et al. (2022); Bao et al. (2021); He et al. (2022); Atito et al. (2021). However, it is challenging

*Correspondence to ho.hin.lee@vanderbilt.edu

to adapt ViT models as generic network backbones due to the high complexity of computing global self-attention with respect to the input size, especially in high resolution images with dense features across scales. Therefore, hierarchical transformers are proposed to bridge these gaps with their intrinsic hybrid structure Zhang et al. (2022); Liu et al. (2021). Introducing the “sliding window” strategy into ViTs termed Swin Transformer behave similarly with ConvNets Liu et al. (2021). In medical domain, SwinUNETR adapts Swin transformer blocks as the generic vision encoder backbone and achieves current state-of-the-art performance for volumetric segmentation Hatamizadeh et al. (2022a). However, a naive implementation of a sliding window for computing self-attention can have a high computation time and bring the system design more sophisticated for efficiency optimization Ramachandran et al. (2019); Liu et al. (2021). As the advancement of ViTs starts to bring back the concepts of convolution, the key components for such large performance differences are attributed to the **scaling behavior** and **global self-attention with large receptive fields**. As such, we further ask: **Can we leverage convolution modules to enable the capabilities of hierarchical transformers?**

Motivated by Liu et al. (2022), who claims to gradually “modernize” a standard ResNet block towards the design of ViTs, we hypothesize that the key attributes for the performance differences between ViTs and ConvNets can be tackled with newly designed convolution blocks, thus enhancing model generalizability for volumetric segmentation. This work explores the essential difference in feature computation and network architecture between 3D ConvNets and hierarchical transformers. Unlike SwinUNETR, we propose a lightweight volumetric ConvNet 3D UX-Net to adapt the intrinsic properties of Swin Transformer with ConvNet modules and enhance the volumetric segmentation performance with smaller model capacities. Specifically, we introduce volumetric depth-wise convolutions with large kernel sizes to simulate the operation of large receptive fields for generating self-attention in Swin transformer. Furthermore, instead of linear scaling the self-attention feature across channels, we further introduce the pointwise depth convolution scaling to distribute each channel-wise feature independently into a wider hidden dimension (e.g., $4 \times \text{input channel}$), thus minimizing the redundancy of learned context across channels and preserving model performances without increasing model capacity. We evaluate 3D UX-Net on supervised volumetric segmentation tasks with three public volumetric datasets: 1) MICCAI Challenge 2021 FeTA (infant brain imaging), 2) MICCAI Challenge 2021 FLARE (abdominal imaging), and 3) MICCAI Challenge 2022 AMOS (abdominal imaging). Surprisingly, 3D UX-Net, a network constructed purely from ConvNet modules, demonstrates a consistent improvement across all datasets comparing with current transformer SOTA. We summarize our contributions as below:

- We propose the 3D UX-Net to adapt transformer behavior purely with ConvNet modules in a volumetric setting. To our best knowledge, this is the first 3D ConvNet architecture that competes favorably with transformers SOTA in volumetric segmentation tasks.
- We leverage depth-wise convolution with large kernel size as the generic feature extraction backbone, and introduce pointwise depth convolution to scale the extracted representations effectively with less parameters.
- We use three challenging public datasets to evaluate 3D UX-Net in 1) direct training and 2) finetuning scenarios with volumetric multi-organ/tissues segmentation. 3D UX-Net achieves consistently improvement in both scenarios across all ConvNets and transformers SOTA with fewer model parameters.

2 RELATED WORK

2.1 TRANSFORMER-BASED SEGMENTATION

Significant efforts have been put into integrating ViTs for dense predictions in medical imaging domain Hatamizadeh et al. (2022b); Chen et al. (2021b); Zhou et al. (2021); Wang et al. (2021a). With the advancement of Swin Transformer, SwinUNETR equips the encoder with the Swin Transformer blocks to compute self-attention for enhancing brain tumor segmentation accuracy in 3D MRI Images Hatamizadeh et al. (2022a). Tang et al. extend the SwinUNETR by adding a self-supervised learning pre-training strategy for fine-tuning segmentation tasks. Another Unet-like architecture Swin-Unet further adapt Swin Transformer on both the encoder and decoder network via skip-connections to learn local and global semantic features for multi-abdominal CT segmenta-

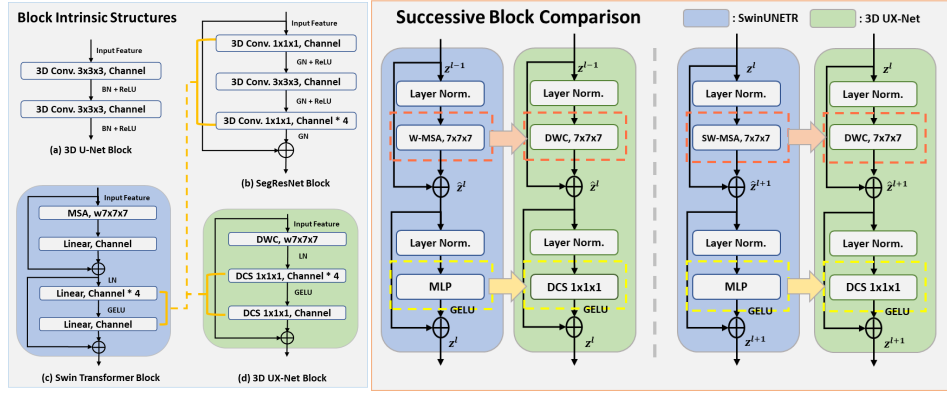


Figure 1: Overview of our proposed designed convolution blocks to simulate the behaviour of swin transformers. We leverage depthwise convolution and pointwise scaling to adapt large receptive field and enrich the features through widening independent channels. We further compare different backbones of volumetric ConvNets and Swin Transformer block architecture. The yellow dotted line demonstrates the differences in spatial position of widening feature channels in the network bottleneck.

tion Cao et al. (2021). Similarly, SwinBTS has the similar intrinsic structure with Swin-Unet with an enhanced transformer module for detailed feature extraction Jiang et al. (2022). However, the transformer-based volumetric segmentation frameworks still require lengthy training time and are accompanied by high computational complexity associated with extracting features at multi-scale levels Xie et al. (2021); Shamshad et al. (2022). Therefore, such limitations motivate us to rethink if ConvNets can emulate transformer behavior to demonstrate efficient feature extraction.

2.2 DEPTHWISE CONVOLUTION BASED SEGMENTATION

Apart from transformer-based framework, previous works began to revisit the concept of depthwise convolution and adapt its characteristics for robust segmentation. It has been proved to be a powerful variation of standard convolution that helps reduce the number of parameters and transfer learning Guo et al. (2019). Zunair et al. introduced an encoder-decoder depth-wise fully convolutional network architecture for lung CT segmentation Zunair & Hamza (2021). 3D U²-Net aims to solve multi-modality segmentation by leveraging depth-wise ConvNet with shared cross-channel correlations, which achieved comparable performance with traditional models but required only about 1% parameters Huang et al. (2019). However, utilizing larger kernel convolution demonstrates the trade-off between search-efficient space and high computation time in 3D ConvNets Tang et al. (2020). Therefore, several works have further investigated the usefulness of large kernel convolution in medical image segmentation. For instance, GCN employs large kernels (5x5, 7x7) for semantic segmentation, which simultaneously addresses the classification and localization problems Peng et al. (2017); Huo et al. integrated large convolutional kernel (7x7) layers and the conditional generative adversarial networks to address the spatial and anatomical variations in splenomegaly segmentation task Huo et al. (2018); ConvUNeXt aims to reduce the training parameters of the convolution block of UNet without trading off model performance with depthwise convolution in 2D Han et al. (2022); Li et al. implemented large kernel convolution to assemble the attention map of long-range relationships on U-Net Li et al. (2022a). Attribute to the potential of depth-wise and large kernel convolution, we hypothesize that combining depth-wise convolution and large kernel size can emulate the transformer behavior to benefit volumetric segmentation.

3 3D UX-NET: INTUITION

Inspired by Liu et al. (2022), we introduce 3D UX-Net, a simple volumetric ConvNet that adapts the capability of hierarchical transformers and preserves the advantages of using ConvNet modules such as inductive biases. The basic idea of designing the encoder block in 3D UX-Net can be divided into

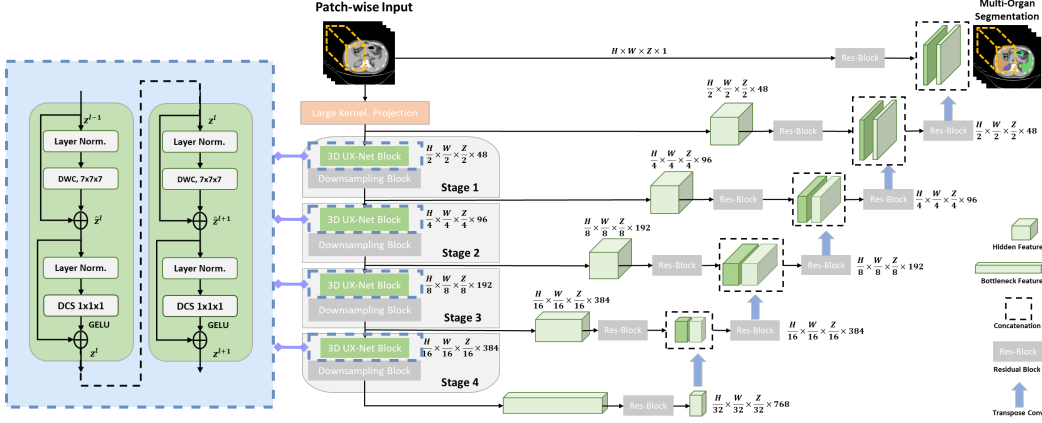


Figure 2: Overview of the proposed 3D UX-Net with our designed convolutional block as the encoder backbone. Large kernel convolution is used to project features into patch-wise embeddings. A downsampling block is used in each stage to mix and enrich context across all channels, while our designed blocks extract meaningful features in depth-wise setting.

1) block-wise and 2) layer-wise perspectives. First, we discuss the block-wise perspective in three views:

- **Patch-wise Features Projection:** Comparing the similarities between ConvNets and ViTs, there is a common block that both networks use to aggressively downscale feature representations into particular patch sizes. Here, instead of flattening image patches as a sequential input with linear layer Dosovitskiy et al. (2020), we adopt a large kernel projection layer to extract patch-wise features as the encoder’s inputs.
- **Volumetric Depth-wise Convolution with Large Kernels:** One of the intrinsic specialties of the swin transformer is the sliding window strategy for computing non-local multi-head self-attention (MSA). Overall, there are two hierarchical ways to compute MSA: 1) window-based MSA (W-MSA) and 2) shifted window MSA (SW-MSA). Both ways generate global receptive field across layers and further refine the feature correspondence between non-overlapping windows. Inspired by the idea of depth-wise convolution, we have found similarities between the weighted sum approach in self-attention and the convolution per-channel basis. We argue that using depth-wise convolution with a large kernel size can provide a large receptive field in extracting features similar to the MSA blocks. Therefore, we propose compressing the window shifting characteristics of the swin transformer with a volumetric depth-wise convolution using a large kernel size (e.g., starting from $7 \times 7 \times 7$). Each kernel channel is convolved with the corresponding input channel, so that the output feature has the same channel dimension as the input.
- **Inverted Bottleneck with Depthwise Convolutional Scaling:** Another intrinsic structure in swin transformer is that they are designed with the hidden dimension of the MLP block to be four times wider than the input dimension, as shown in Figure 1. Such a design is interestingly correlated to the expansion ratio in the ResNet block He et al. (2016). Therefore, we leverage the similar design in ResNet block and move up the depth-wise convolution to compute features. Furthermore, we introduce depthwise convolutional scaling (DCS) with $1 \times 1 \times 1$ kernel to linearly scale each channel feature independently. We enrich the feature representations by expanding and compressing each channel independently, thus minimizing the redundancy of cross-channel context. We enhance the cross-channel feature correspondences with the downsampling block in each stage. By using DCS, we further reduce the model complexity by 5% and demonstrates a comparable results with the block architecture using MLP.

The macro-design in convolution blocks demonstrates the possibility of adapting the large receptive field and leveraging similar operation of extracting features compared with the swin transformer. We want to further investigate the variation between ConvNets and the swin transformer in layer-wise

settings and refine the model architecture to better simulate ViTs in macro-level. Here, we further define and adapt layer-wise differences into another three perspectives:

- **Applying Residual Connections:** From Figure 1, the golden standard 3D U-Net block demonstrates the naive approach of using small kernels to extract local representations with increased channels Çiçek et al. (2016), while the SegResNet block applies the residual similar to the transformer block Myronenko (2018). Here, we also apply residual connections between the input and the extracted features after the last scaling layer. However, we do not apply any normalization and activation layers before and after the summation of residual to be equivalent with the swin transformer structure.
- **Adapting Layer Normalization (LN):** In ConvNets, batch normalization (BN) is a common strategy that normalizes convolved representations to enhance convergence and reduce overfitting. However, previous works have demonstrated that BN can lead to a detrimental effect in model generalizability Wu & Johnson (2021). Although several approaches have been proposed to have an alternative normalization techniques Salimans & Kingma (2016); Ulyanov et al. (2016); Wu & He (2018), BN still remains as the optimal choice in volumetric vision tasks. Motivated by vision transformers and Liu et al. (2022), we directly substitute BN with LN in the encoder block and demonstrate similar operations in ViTs Ba et al. (2016).
- **Using GELU as the Activation Layer:** Many previous works have used the rectified linear unit (ReLU) activation layers Nair & Hinton (2010), providing non-linearity in both ConvNets and ViTs. However, previously proposed transformer models demonstrate the Gaussian error linear unit (GELU) to be a smoother variant, which tackle the limitation of sudden zero in the negative input range in ReLU Hendrycks & Gimpel (2016). Therefore, we further substitute the ReLU with the GELU activation function.

4 3D UX-NET: COMPLETE NETWORK DESCRIPTION

3D UX-Net comprises multiple re-designed volumetric convolution blocks that directly utilize 3D patches. Skip connections are further leveraged to connect the multi-resolution features to a convolution-based decoder network. Figure 2 illustrates the complete architecture of 3D UX-Net. We further describe the details of the encoder and decoder in this section.

4.1 DEPTH-WISE CONVOLUTION ENCODER

Given a set of 3D image volumes $V_i = X_i, Y_{i=1, \dots, L}$, random sub-volumes $P_i \in \mathcal{R}^{H \times W \times D \times C}$ are extracted to be the inputs for the encoder network. Instead of flattening the patches and projecting it with linear layer Hatamizadeh et al. (2022b), we leverage a large kernel convolutional layer to compute partitioned feature map with size $\frac{H}{2} \times \frac{W}{2} \times \frac{D}{2}$ that are projected into a $C = 48$ -dimensional space. To adapt the characteristics of computing local self-attention, we use the depthwise convolution with kernel size starting from $7 \times 7 \times 7$ (DWC) with padding of 3, to act as a "shifted window" and evenly divide the feature map. As global self-attention is generally not computationally affordable with a large number of patches extracted in the Swin Transformer Liu et al. (2021), we hypothesize that performing depthwise convolution with a large kernel size can effectively extract features with a global receptive field. Therefore, we define the output of encoder blocks in layers l and $l + 1$ as follows:

$$\begin{aligned}\hat{z}^l &= \text{DWC}(\text{LN}(z^{l-1})) + z^{l-1} \\ z^l &= \text{DCS}(\text{LN}(\hat{z}^l)) + \hat{z}^l \\ \hat{z}^{l+1} &= \text{DWC}(\text{LN}(z^l)) + z^l \\ z^{l+1} &= \text{DCS}(\text{LN}(\hat{z}^{l+1})) + \hat{z}^{l+1}\end{aligned}\tag{1}$$

where \hat{z}_l and \hat{z}_{l+1} are the outputs from the DWC layer in different depth levels; LN and DCS denote as the layer normalization and the depthwise convolution scaling, respectively (see. Figure 1). Compared to the swin transformer, we substitute the regular and window partitioning multi-head self-attention modules, W-MSA and SW-MSA respectively, with two DWC layers.

Motivated by SwinUNETR Tang et al. (2022); Hatamizadeh et al. (2022a), the complete architecture of the encoder consists of 4 stages comprising of 2 large kernel convolution blocks at each stage (*i.e.*

Table 1: Comparison of transformer and ConvNet SOTA approaches on the Feta 2021 and FLARE 2021 testing dataset. (*: $p < 0.01$, with Wilcoxon signed-rank test to all SOTA approaches)

| Methods | #Params | FLOPs | FeTA 2021 | | | | | | | | FLARE 2021 | | | | |
|--------------------------------------|--------------|---------------|--------------|--------------|--------------|--------------|--------------|--------------|--------------|---------------|--------------|--------------|--------------|--------------|---------------|
| | | | ECF | GM | WM | Vent. | Cereb. | DGM | BS | Mean | Spleen | Kidney | Liver | Pancreas | Mean |
| 3D U-Net Çiçek et al. (2016) | 4.81M | 135.9G | 0.867 | 0.762 | 0.925 | 0.861 | 0.910 | 0.845 | 0.827 | 0.857 | 0.911 | 0.962 | 0.905 | 0.789 | 0.892 |
| SegResNet Myronenko (2018) | 1.18M | 15.6G | 0.868 | 0.770 | 0.927 | 0.865 | 0.911 | 0.867 | 0.825 | 0.862 | 0.963 | 0.934 | 0.965 | 0.745 | 0.902 |
| RAP-Net Lee et al. (2021) | 38.2M | 101.2G | 0.880 | 0.771 | 0.927 | 0.862 | 0.907 | 0.879 | 0.832 | 0.865 | 0.946 | 0.967 | 0.940 | 0.799 | 0.913 |
| nn-UNet Isensee et al. (2021) | 31.2M | 743.3G | 0.883 | 0.775 | 0.930 | 0.868 | 0.920 | 0.880 | 0.840 | 0.870 | 0.971 | 0.966 | 0.976 | 0.792 | 0.926 |
| TransBTS Wang et al. (2021a) | 31.6M | 110.4G | 0.885 | 0.778 | 0.932 | 0.861 | 0.913 | 0.876 | 0.837 | 0.868 | 0.964 | 0.959 | 0.974 | 0.711 | 0.902 |
| UNETR Hatamizadeh et al. (2022b) | 92.8M | 82.6G | 0.861 | 0.762 | 0.927 | 0.862 | 0.908 | 0.868 | 0.834 | 0.860 | 0.927 | 0.947 | 0.960 | 0.710 | 0.886 |
| nnFormer Zhou et al. (2021) | 149.3M | 240.2G | 0.880 | 0.770 | 0.930 | 0.857 | 0.903 | 0.876 | 0.828 | 0.863 | 0.973 | 0.960 | 0.975 | 0.717 | 0.906 |
| SwinUNETR Hatamizadeh et al. (2022a) | 62.2M | 328.4G | 0.873 | 0.772 | 0.929 | 0.869 | 0.914 | 0.875 | 0.842 | 0.867 | 0.979 | 0.965 | 0.980 | 0.788 | 0.929 |
| 3D UX-Net (Ours) | 53.0M | 639.4G | 0.882 | 0.780 | 0.934 | 0.872 | 0.917 | 0.886 | 0.845 | 0.874* | 0.981 | 0.969 | 0.982 | 0.801 | 0.934* |

Table 2: Comparison of Finetuning performance with transformer SOTA approaches on the AMOS 2021 testing dataset. (*: $p < 0.01$, with Wilcoxon signed-rank test to all SOTA approaches)

| Methods | Spleen | R. Kid | L. Kid | Gall. | Eso. | Liver | Stom. | Aorta | IVC | Panc. | RAG | LAG | Duo. | Blad. | Pros. | Avg |
|------------------|--------------|--------------|--------------|--------------|--------------|--------------|--------------|--------------|--------------|--------------|--------------|--------------|--------------|--------------|--------------|---------------|
| TransBTS | 0.885 | 0.931 | 0.916 | 0.817 | 0.744 | 0.969 | 0.837 | 0.914 | 0.855 | 0.724 | 0.630 | 0.566 | 0.704 | 0.741 | 0.650 | 0.792 |
| UNETR | 0.926 | 0.936 | 0.918 | 0.785 | 0.702 | 0.969 | 0.788 | 0.893 | 0.828 | 0.732 | 0.717 | 0.554 | 0.658 | 0.683 | 0.722 | 0.762 |
| nnFormer | 0.935 | 0.904 | 0.887 | 0.836 | 0.712 | 0.964 | 0.798 | 0.901 | 0.821 | 0.734 | 0.665 | 0.587 | 0.641 | 0.744 | 0.714 | 0.790 |
| SwinUNETR | 0.959 | 0.960 | 0.949 | 0.894 | 0.827 | 0.979 | 0.899 | 0.944 | 0.899 | 0.828 | 0.791 | 0.745 | 0.817 | 0.875 | 0.841 | 0.880 |
| 3D UX-Net | 0.970 | 0.967 | 0.961 | 0.923 | 0.832 | 0.984 | 0.920 | 0.951 | 0.914 | 0.856 | 0.825 | 0.739 | 0.853 | 0.906 | 0.876 | 0.900* |

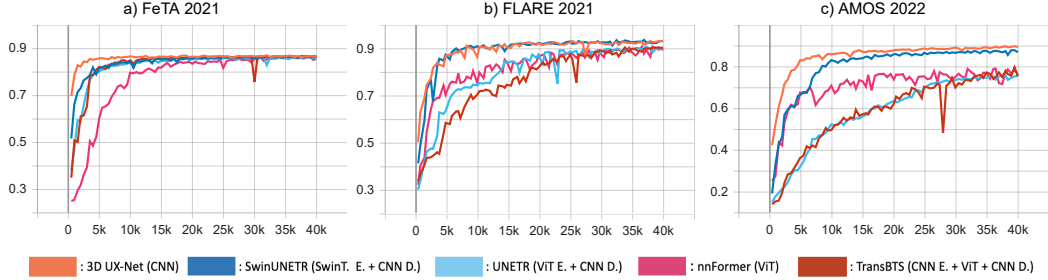


Figure 3: Validation Curve with Dice Score for FeTA2021 (a), FLARE2021 (b) and AMOS2022 (c). 3D UX-Net demonstrates the fastest convergence rate with limited samples training (FeTA2021) and transfer learning (AMOS2022) scenario respectively, while the convergence rate is comparable to SwinUNETR with the increase of sample size training (FLARE2021).

L=8 total layers). Inside the block, the DCS layer is followed by the DWC layer in each block. The DCS layer helps scale the dimension of the feature map (4 times of the input channel size) without increasing model parameters and minimizes the redundancy of the learned volumetric context across channels. To exchange the information across channels, instead of using MLP, we leverage a standard convolution block with kernel size $2 \times 2 \times 2$ with stride 2 to downscale the feature resolution by a factor of 2. The same procedure continues in stage 2, stage 3 and stage 4 with the resolutions of $\frac{H}{4} \times \frac{W}{4} \times \frac{D}{4}$, $\frac{H}{8} \times \frac{W}{8} \times \frac{D}{8}$ and $\frac{H}{16} \times \frac{W}{16} \times \frac{D}{16}$ respectively. Such hierarchical representations in multi-scale setting are extracted in each stage and are further leveraged for learning dense volumetric segmentation.

4.2 DECODER

The multi-scale output from each stage in the encoder is connected to a ConvNet-based decoder via skip connections and form a "U-shaped" like network for downstream segmentation task. Specifically, we extract the output feature mapping of each stage i ($i \in 0, 1, 2, 3, 4$) in the encoder and further leverage a residual block comprising two post-normalized $3 \times 3 \times 3$ convolutional layers with instance normalization to stabilize the extracted features. The processed features from each stage are then upsampled with a transpose convolutional layer and concatenated with the features from the preceding stage. For downstream volumetric segmentation, we also concatenate the residual features from the input patches with the upsampled features and input the features into a residual block with $1 \times 1 \times 1$ convolutional layer with a softmax activation to predict the segmentation probabilities.

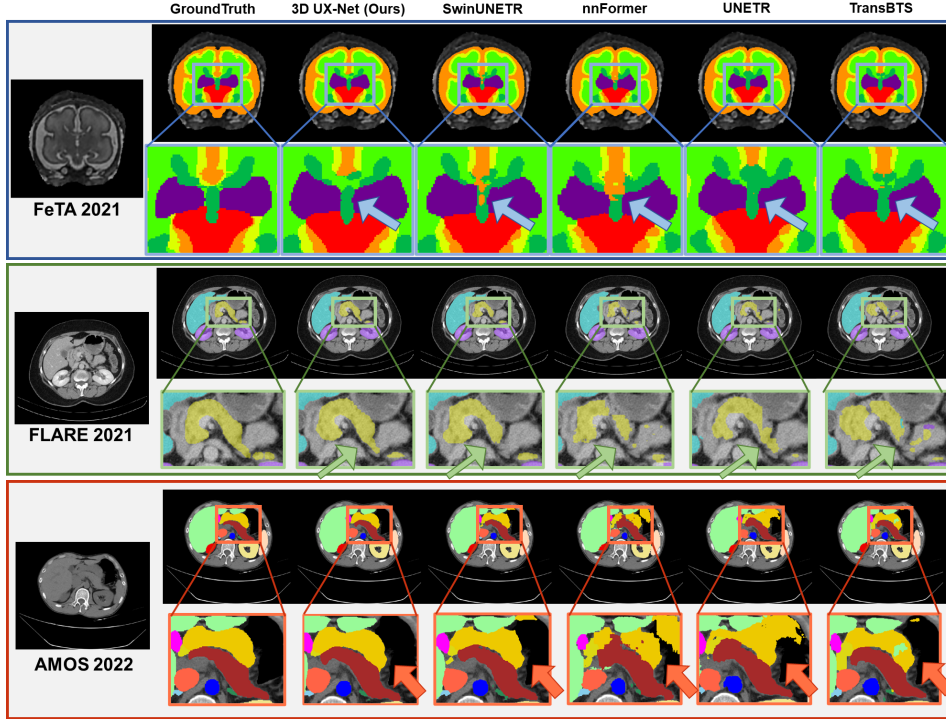


Figure 4: Qualitative representations of tissues and multi-organ segmentation across three public datasets. Boxed are further zoomed in and visualize the significant differences in segmentation quality. 3D UX-Net shows the best segmentation quality compared to the ground-truth.

5 EXPERIMENTAL SETUP

Datasets We conduct experiments on three public multi-modality datasets for volumetric segmentation, which comprising with 1) MICCAI 2021 FeTA Challenge dataset (FeTA2021) Payette et al. (2021), 2) MICCAI 2021 FLARE Challenge dataset (FLARE2021) Ma et al. (2021), and 3) MICCAI 2022 AMOS Challenge dataset (AMOS2022) Ji et al. (2022). For the FETA2021 dataset, we employ 80 T2-weighted infant brain MRIs from the University Children’s Hospital with 1.5 T and 3T clinical whole-body scanners for brain tissue segmentation, with seven specific tissues well-annotated. For FLARE2021 and AMOS2022, we employ 511 multi-contrast abdominal CT from FLARE2021 with four anatomies manually annotated and 200 multi-contrast abdominal CT from AMOS 2022 with sixteen anatomies manually annotated for abdominal multi-organ segmentation. More details of the three public datasets can be found in appendix A.2.

Implementation Details We perform evaluations on two scenarios: 1) direct supervised training and 2) transfer learning with pretrained weights. FeTA2021 and FLARE2021 datasets are leverage to evaluate in direct training scenario, while AMOS dataset is used in transfer learning scenario. We perform five-fold cross-validations with 80% (train)/ 10% (validation)/ 10% (test) split to both FeTA2021 and FLARE2021 datasets. For the transfer learning scenario, we leverage the pretrained weights from the best fold model trained with FLARE2021, and finetune the model weights on AMOS2022 to evaluate the fine-tuning capability of 3D UX-Net, with the the same train/validation/test split. The complete preprocessing and training details are available at the appendix A.1. Overall, we evaluate 3D UX-Net performance by comparing with current volumetric transformer and ConvNet SOTA approaches for volumetric segmentation in fully-supervised setting. We use the Dice similarity coefficient as an evaluation metric to compare the overlapping regions between predictions and ground-truth labels. Furthermore, we performed ablation studies to investigate the effect on different kernel size and the variability of substituting linear layers with depthwise convolution for feature extraction.

Table 3: Ablation studies of different architecture on FeTA2021 and FLARE2021

| Methods | #Params (M) | FeTA2021 Mean Dice | FLARE2021 Mean Dice |
|----------------------------------|-------------|-----------------------|------------------------|
| SwinUNETR | 62.2 | 0.867 | 0.929 |
| Use Standard Conv. | 186.9 | 0.875 | 0.937 |
| Use Depth Conv. | 53.0 | 0.874 | 0.934 |
| Kernel= $7 \times 7 \times 7$ | 53.0 | 0.874 | 0.934 |
| Kernel= $9 \times 9 \times 9$ | 53.6 | 0.870 | 0.934 |
| Kernel= $11 \times 11 \times 11$ | 54.4 | 0.871 | 0.936 |
| Kernel= $13 \times 13 \times 13$ | 55.7 | 0.871 | 0.938 |
| No MLP | 51.1 | 0.869 | 0.915 |
| Use MLP | 56.3 | 0.872 | 0.933 |
| Use DCS $1 \times 1 \times 1$ | 53.0 | 0.874 | 0.934 |

6 RESULTS

In this section, we first perform evaluation to our proposed network 3D UX-Net with training from scratch setting, using FeTA 2021 dataset and FLARE 2021 dataset. We then evaluate transfer learning capability of 3D UX-Net by leveraging the best fold of FLARE2021-trained model as pretrain weights, and finetune on AMOS 2022 dataset for multi-organ segmentation.

6.1 EVALUATION ON FETA & FLARE

Table 1 shows the result comparison of current transformers and ConvNets SOTA on medical image segmentation in volumetric setting. With our designed convolutional blocks as the encoder backbone, 3D UX-Net demonstrates the best performance across all segmentation task with significant improvement in Dice score (FeTA2021: 0.870 to 0.874, FLARE2021: 0.929 to 0.934). From Figure 2, we observe that 3D UX-Net demonstrates the quickest convergence rate in training with FeTA2021 datasets. Interestingly, when the training sample size increases, the efficiency of training convergence starts to become compatible between SwinUNETR and 3D UX-Net. Apart from the quantitative representations, Figure 3 further provides additional confidence of demonstrating the quality improvement in segmentation with 3D UX-Net. The morphology of organs and tissues are well preserved compared to the ground-truth label.

6.2 TRANSFER LEARNING WITH AMOS

Apart from training from scratch scenario, we further investigate the transfer learning capability of 3D UX-Net comparing to the transformers SOTA with AMOS 2022 dataset. We observe that the finetuning performance of 3D UX-Net significantly outperforms other transformer network with mean Dice of 0.900 (2.27% enhancement) and most of the organs segmentation demonstrate a consistent improvement in quality. Also, from Figure 2, although the convergence curve of each transformer network shows the comparability to that of the FLARE2021-trained model, 3D UX-Net further shows its capability in adapting fast convergence and enhancing the robustness of the model with finetuning. Furthermore, the qualitative representations in Figure 3 demonstrates a significant improvement in preserving boundaries between neighboring organs and minimize the possibility of over-segmentation towards other organ regions.

6.3 ABLATION ANALYSIS

After evaluating the core performance of 3D UX-Net, we study how the different components in our designed architecture contribute to such a significant improvement in performance, as well as how they interact with other components. Here, both FeTA2021 and FLARE2021 are leveraged to perform ablation studies towards different modules. All ablation studies are performed with kernel size $7 \times 7 \times 7$ scenario except the study of evaluating the variability of kernel size.

Comparing with Standard Convolution: We investigate the effectiveness of both standard convo-

lution and depthwise convolution for initial feature extraction. With the use of standard convolution, it demonstrates a slight improvement with standard convolution. However, the model parameters are about 3.5 times than that of using depthwise convolution, while the segmentation performance with depthwise convolution still demonstrates a comparable performance in both datasets.

Variation of Kernel Size: From Table 3, we observe that the convolution with kernel size $7 \times 7 \times 7$ optimally works for FeTA2021 dataset, while the segmentation performance of FLARE2021 demonstrates the best with kernel size of $13 \times 13 \times 13$. The significant improvement of using $13 \times 13 \times 13$ kernel for FLARE2021 may be due to the larger receptive field provided to enhance the feature correspondence between multiple neighboring organs within the abdominal region. For FeTA2021 dataset, only the small infant brains are well localized as foreground and $7 \times 7 \times 7$ kernel demonstrates to be optimal receptive field to extract the tissues correspondence.

Adapting DCS: We found that a significant decrement is performed without using MLP for feature scaling. With the linear scaling, the performance enhanced significantly in FLARE2021, while a slight improvement is demonstrated in FeTA2021. Interestingly, leveraging depthwise convolution with $1 \times 1 \times 1$ kernel size for scaling, demonstrates a slightly enhancement in performance for both FeTA2021 and FLARE2021 datasets. Also, the model parameters further drops from 56.3M to 53.0M without trading off the model performance.

7 DISCUSSION

In this work, we present a block-wise design to simulate the behavior of swin transformers using pure ConvNet modules. We further adapt our design as a generic encoder backbone into "U-Net" like architecture via skip connections for volumetric segmentation. We found that the key components for improved performance can be divided into two main perspectives: 1) the sliding window strategy of computing multi-head self-attention (MSA) and 2) the inverted bottleneck architecture of widening the computed feature channels. The W-MSA enhances learning the feature correspondence within each window, while the SW-MSA strengthens the cross-window connections at the feature level between different non-overlapping windows. Such strategy integrates ConvNet priors into transformer networks and enlarge receptive fields for feature extraction. However, we found that the depth convolutions can demonstrate similar operations of computing MSA in Swin Transformer blocks. In depth-wise convolutions, we convolve each input channel with a single convolutional filter and stack the convolved outputs together, which is comparable to the patch merging layer for feature outputs in swin transformers. Furthermore, adapting the depth convolutions with large kernel filters demonstrates similarities with both W-MSA and SW-MSA, which learns the feature connections within a large receptive field. Our design provides similar capabilities to Swin Transformer and additionally has the advantage of reducing the number of model parameters using ConvNet modules.

Another interesting difference is the inverted bottleneck architecture. Figure 1 shows that both Swin Transformers and some standard ConvNets have their specific bottleneck architectures (yellow dotted line). The distinctive component in swin transformer's bottleneck is to maintain the channels size as four times wider than the input dimension and the spatial position of the MSA layer. We follow the inverted bottleneck architecture in Swin Transformer block and move the depthwise convolution to the top similar to the MSA layer. Instead of using linear scaling, we introduce the idea of depthwise convolution in pointwise setting to scale the dense feature with wider channels. Interestingly, we found a slight improvement in performance is shown across datasets (FeTA2021: 0.872 to 0.874, FLARE2021: 0.933 to 0.934), but with less model parameters. As each encoder block only consists of two scaling layers, the limited number of scaling blocks may affect the performance to a small extent. We will further investigate the scalability of linear scaling layer in 3D as the future work.

8 CONCLUSION

We introduce 3D UX-Net, the first volumetric network adapting the capabilities of hierarchical transformer with pure ConvNet modules for medical image segmentation. We re-design the encoder blocks with depthwise convolution and projections to simulate the behavior of hierarchical transformer. Furthermore, we adjust layer-wise design in the encoder block and enhance the segmentation performance across different training settings. 3D UX-Net outperforms current transformer SOTAs with fewer model parameters using three challenging public datasets in both supervised training and transfer learning scenarios.

ACKNOWLEDGMENTS

This research is supported by NIH Common Fund and National Institute of Diabetes, Digestive and Kidney Diseases U54DK120058 (Spraggins), NSF CAREER 1452485, NIH 2R01EB006136, NIH 1R01EB017230 (Landman), and NIH R01NS09529. This study was in part using the resources of the Advanced Computing Center for Research and Education (ACCRE) at Vanderbilt University, Nashville, TN. The identified datasets used for the analysis described were obtained from the Research Derivative (RD), database of clinical and related data. The imaging dataset(s) used for the analysis described were obtained from ImageVU, a research repository of medical imaging data and image-related metadata. ImageVU and RD are supported by the VICTR CTSA award (ULTR000445 from NCATS/NIH) and Vanderbilt University Medical Center institutional funding. ImageVU pilot work was also funded by PCORI (contract CDRN-1306-04869).

REFERENCES

- Sara Atito, Muhammad Awais, and Josef Kittler. Sit: Self-supervised vision transformer. *arXiv preprint arXiv:2104.03602*, 2021.
- Jimmy Lei Ba, Jamie Ryan Kiros, and Geoffrey E Hinton. Layer normalization. *arXiv preprint arXiv:1607.06450*, 2016.
- Hangbo Bao, Li Dong, and Furu Wei. Beit: Bert pre-training of image transformers. *arXiv preprint arXiv:2106.08254*, 2021.
- Srinadh Bhojanapalli, Ayan Chakrabarti, Daniel Glasner, Daliang Li, Thomas Unterthiner, and Andreas Veit. Understanding robustness of transformers for image classification. In *Proceedings of the IEEE/CVF International Conference on Computer Vision*, pp. 10231–10241, 2021.
- Hu Cao, Yueyue Wang, Joy Chen, Dongsheng Jiang, Xiaopeng Zhang, Qi Tian, and Manning Wang. Swin-unet: Unet-like pure transformer for medical image segmentation. *arXiv preprint arXiv:2105.05537*, 2021.
- Chun-Fu Richard Chen, Quanfu Fan, and Rameswar Panda. Crossvit: Cross-attention multi-scale vision transformer for image classification. In *Proceedings of the IEEE/CVF international conference on computer vision*, pp. 357–366, 2021a.
- Jieneng Chen, Yongyi Lu, Qihang Yu, Xiangde Luo, Ehsan Adeli, Yan Wang, Le Lu, Alan L Yuille, and Yuyin Zhou. Transunet: Transformers make strong encoders for medical image segmentation. *arXiv preprint arXiv:2102.04306*, 2021b.
- Özgün Çiçek, Ahmed Abdulkadir, Soeren S Lienkamp, Thomas Brox, and Olaf Ronneberger. 3d unet: learning dense volumetric segmentation from sparse annotation. In *International conference on medical image computing and computer-assisted intervention*, pp. 424–432. Springer, 2016.
- Alexey Dosovitskiy, Lucas Beyer, Alexander Kolesnikov, Dirk Weissenborn, Xiaohua Zhai, Thomas Unterthiner, Mostafa Dehghani, Matthias Minderer, Georg Heigold, Sylvain Gelly, et al. An image is worth 16x16 words: Transformers for image recognition at scale. *arXiv preprint arXiv:2010.11929*, 2020.
- Yunhui Guo, Yandong Li, Liqiang Wang, and Tajana Rosing. Depthwise convolution is all you need for learning multiple visual domains. In *Proceedings of the AAAI Conference on Artificial Intelligence*, volume 33, pp. 8368–8375, 2019.
- Zhimeng Han, Muwei Jian, and Gai-Ge Wang. Convunext: An efficient convolution neural network for medical image segmentation. *Knowledge-Based Systems*, pp. 109512, 2022.
- Ali Hatamizadeh, Vishwesh Nath, Yucheng Tang, Dong Yang, Holger R Roth, and Daguang Xu. Swin unetr: Swin transformers for semantic segmentation of brain tumors in mri images. In *International MICCAI Brainlesion Workshop*, pp. 272–284. Springer, 2022a.
- Ali Hatamizadeh, Yucheng Tang, Vishwesh Nath, Dong Yang, Andriy Myronenko, Bennett Landman, Holger R Roth, and Daguang Xu. Unetr: Transformers for 3d medical image segmentation. In *Proceedings of the IEEE/CVF Winter Conference on Applications of Computer Vision*, pp. 574–584, 2022b.

- Kaiming He, Xiangyu Zhang, Shaoqing Ren, and Jian Sun. Deep residual learning for image recognition. In *Proceedings of the IEEE conference on computer vision and pattern recognition*, pp. 770–778, 2016.
- Kaiming He, Xinlei Chen, Saining Xie, Yanghao Li, Piotr Dollár, and Ross Girshick. Masked autoencoders are scalable vision learners. In *Proceedings of the IEEE/CVF Conference on Computer Vision and Pattern Recognition*, pp. 16000–16009, 2022.
- Dan Hendrycks and Kevin Gimpel. Gaussian error linear units (gelus). *arXiv preprint arXiv:1606.08415*, 2016.
- Chao Huang, Hu Han, Qingsong Yao, Shankuan Zhu, and S Kevin Zhou. 3d u^2 -net: A 3d universal u-net for multi-domain medical image segmentation. In *International Conference on Medical Image Computing and Computer-Assisted Intervention*, pp. 291–299. Springer, 2019.
- Yuankai Huo, Zhoubing Xu, Shunxing Bao, Camilo Bermudez, Hyeonsoo Moon, Prasanna Parvathaneni, Tamara K Moyo, Michael R Savona, Albert Assad, Richard G Abramson, et al. Splenomegaly segmentation on multi-modal mri using deep convolutional networks. *IEEE transactions on medical imaging*, 38(5):1185–1196, 2018.
- Fabian Isensee, Paul F Jaeger, Simon AA Kohl, Jens Petersen, and Klaus H Maier-Hein. nnu-net: a self-configuring method for deep learning-based biomedical image segmentation. *Nature methods*, 18(2):203–211, 2021.
- Yuanfeng Ji, Haotian Bai, Jie Yang, Chongjian Ge, Ye Zhu, Ruimao Zhang, Zhen Li, Lingyan Zhang, Wanling Ma, Xiang Wan, et al. Amos: A large-scale abdominal multi-organ benchmark for versatile medical image segmentation. *arXiv preprint arXiv:2206.08023*, 2022.
- Yun Jiang, Yuan Zhang, Xin Lin, Jinkun Dong, Tongtong Cheng, and Jing Liang. Swinbts: a method for 3d multimodal brain tumor segmentation using swin transformer. *Brain Sciences*, 12(6):797, 2022.
- Ho Hin Lee, Yucheng Tang, Shunxing Bao, Richard G Abramson, Yuankai Huo, and Bennett A Landman. Rap-net: Coarse-to-fine multi-organ segmentation with single random anatomical prior. In *2021 IEEE 18th International Symposium on Biomedical Imaging (ISBI)*, pp. 1491–1494. IEEE, 2021.
- Hao Li, Yang Nan, and Guang Yang. Lkai-net: 3d large-kernel attention-based u-net for automatic mri brain tumor segmentation. In *Annual Conference on Medical Image Understanding and Analysis*, pp. 313–327. Springer, 2022a.
- Yanghao Li, Chao-Yuan Wu, Haoqi Fan, Karttikeya Mangalam, Bo Xiong, Jitendra Malik, and Christoph Feichtenhofer. Mvitv2: Improved multiscale vision transformers for classification and detection. In *Proceedings of the IEEE/CVF Conference on Computer Vision and Pattern Recognition*, pp. 4804–4814, 2022b.
- Ze Liu, Yutong Lin, Yue Cao, Han Hu, Yixuan Wei, Zheng Zhang, Stephen Lin, and Baining Guo. Swin transformer: Hierarchical vision transformer using shifted windows. In *Proceedings of the IEEE/CVF International Conference on Computer Vision*, pp. 10012–10022, 2021.
- Zhuang Liu, Hanzi Mao, Chao-Yuan Wu, Christoph Feichtenhofer, Trevor Darrell, and Saining Xie. A convnet for the 2020s. In *Proceedings of the IEEE/CVF Conference on Computer Vision and Pattern Recognition*, pp. 11976–11986, 2022.
- Jun Ma, Yao Zhang, Song Gu, Cheng Zhu, Cheng Ge, Yichi Zhang, Xingle An, Congcong Wang, Qiyuan Wang, Xin Liu, et al. Abdomenct-1k: Is abdominal organ segmentation a solved problem. *IEEE Transactions on Pattern Analysis and Machine Intelligence*, 2021.
- Andriy Myronenko. 3d mri brain tumor segmentation using autoencoder regularization. In *International MICCAI Brainlesion Workshop*, pp. 311–320. Springer, 2018.
- Vinod Nair and Geoffrey E Hinton. Rectified linear units improve restricted boltzmann machines. In *Icml*, 2010.

- Kelly Payette, Priscille de Dumast, Hamza Kebiri, Ivan Ezhov, Johannes C Paetzold, Suprosanna Shit, Asim Iqbal, Romesa Khan, Raimund Kottke, Patrice Grethen, et al. An automatic multi-tissue human fetal brain segmentation benchmark using the fetal tissue annotation dataset. *Scientific Data*, 8(1):1–14, 2021.
- Chao Peng, Xiangyu Zhang, Gang Yu, Guiming Luo, and Jian Sun. Large kernel matters—improve semantic segmentation by global convolutional network. In *Proceedings of the IEEE conference on computer vision and pattern recognition*, pp. 4353–4361, 2017.
- Prajit Ramachandran, Niki Parmar, Ashish Vaswani, Irwan Bello, Anselm Levskaya, and Jon Shlens. Stand-alone self-attention in vision models. *Advances in Neural Information Processing Systems*, 32, 2019.
- Tim Salimans and Durk P Kingma. Weight normalization: A simple reparameterization to accelerate training of deep neural networks. *Advances in neural information processing systems*, 29, 2016.
- Fahad Shamshad, Salman Khan, Syed Waqas Zamir, Muhammad Haris Khan, Munawar Hayat, Fahad Shahbaz Khan, and Huazhu Fu. Transformers in medical imaging: A survey. *arXiv preprint arXiv:2201.09873*, 2022.
- Haotian Tang, Zhijian Liu, Shengyu Zhao, Yujun Lin, Ji Lin, Hanrui Wang, and Song Han. Searching efficient 3d architectures with sparse point-voxel convolution. In *European conference on computer vision*, pp. 685–702. Springer, 2020.
- Yucheng Tang, Dong Yang, Wenqi Li, Holger R Roth, Bennett Landman, Daguang Xu, Vishwesh Nath, and Ali Hatamizadeh. Self-supervised pre-training of swin transformers for 3d medical image analysis. In *Proceedings of the IEEE/CVF Conference on Computer Vision and Pattern Recognition*, pp. 20730–20740, 2022.
- Dmitry Ulyanov, Andrea Vedaldi, and Victor Lempitsky. Instance normalization: The missing ingredient for fast stylization. *arXiv preprint arXiv:1607.08022*, 2016.
- Wenxuan Wang, Chen Chen, Meng Ding, Hong Yu, Sen Zha, and Jiangyun Li. Transbts: Multimodal brain tumor segmentation using transformer. In *International Conference on Medical Image Computing and Computer-Assisted Intervention*, pp. 109–119. Springer, 2021a.
- Xiyue Wang, Sen Yang, Jun Zhang, Minghui Wang, Jing Zhang, Junzhou Huang, Wei Yang, and Xiao Han. Transpath: Transformer-based self-supervised learning for histopathological image classification. In *International Conference on Medical Image Computing and Computer-Assisted Intervention*, pp. 186–195. Springer, 2021b.
- Yuxin Wu and Kaiming He. Group normalization. In *Proceedings of the European conference on computer vision (ECCV)*, pp. 3–19, 2018.
- Yuxin Wu and Justin Johnson. Rethinking” batch” in batchnorm. *arXiv preprint arXiv:2105.07576*, 2021.
- Yutong Xie, Jianpeng Zhang, Chunhua Shen, and Yong Xia. Cotr: Efficiently bridging cnn and transformer for 3d medical image segmentation. In *International conference on medical image computing and computer-assisted intervention*, pp. 171–180. Springer, 2021.
- Shuang Yu, Kai Ma, Qi Bi, Cheng Bian, Munan Ning, Nanjun He, Yuexiang Li, Hanruo Liu, and Yefeng Zheng. Mil-vt: Multiple instance learning enhanced vision transformer for fundus image classification. In *International Conference on Medical Image Computing and Computer-Assisted Intervention*, pp. 45–54. Springer, 2021.
- Zizhao Zhang, Han Zhang, Long Zhao, Ting Chen, Sercan Ö Arik, and Tomas Pfister. Nested hierarchical transformer: Towards accurate, data-efficient and interpretable visual understanding. In *Proceedings of the AAAI Conference on Artificial Intelligence*, volume 36, pp. 3417–3425, 2022.
- Hong-Yu Zhou, Jiansen Guo, Yinghao Zhang, Lequan Yu, Liansheng Wang, and Yizhou Yu. nn-former: Interleaved transformer for volumetric segmentation. *arXiv preprint arXiv:2109.03201*, 2021.

Hasib Zunair and A Ben Hamza. Sharp u-net: depthwise convolutional network for biomedical image segmentation. *Computers in Biology and Medicine*, 136:104699, 2021.

A APPENDIX

A.1 DATA PREPROCESSING & MODEL TRAINING

We apply hierarchical steps for data preprocessing: 1) intensity clipping is applied to further enhance the contrast of soft tissue (FLARE2021 & AMOS2022: {min:-175, max:250}). 2) Intensity normalization is performed after clipping for each volume and use min-max normalization: $(X - X_1)/(X_{99} - X_1)$ to normalize the intensity value between 0 and 1, where X_p denote as the p_{th} percentile of intensity in X . We then randomly crop sub-volumes with size $96 \times 96 \times 96$ at the foreground and perform data augmentations, including rotations, intensity shifting, and scaling (scaling factor: 0.1). All training processes with 3D UX-Net are optimized with an AdamW optimizer. We trained all models for 40000 steps using a learning rate of 0.0001 on an NVIDIA-Quadro RTX 5000 for both FeTA2021 and FLARE2021, while we perform training for AMOS2022 using NVIDIA-Quadro RTX A6000. One epoch takes approximately about 1 minute for FeTA2021, 10 minutes for FLARE2021, and 7 minutes for AMOS2022, respectively. We further summarize all the training parameters with Table 4.

Table 4: Hyperparameters of both directly training and finetuning scenarios on three public datasets

| Hyperparameters | Direct Training | Finetuning |
|----------------------------|------------------------------------|------------|
| Encoder Stage | 4 | |
| Layer-wise Channel | 48, 96, 192, 384 | |
| Hidden Dimensions | 768 | |
| Patch Size | $96 \times 96 \times 96$ | |
| No. of Sub-volumes Cropped | 2 | 1 |
| Training Steps | 40000 | |
| Batch Size | 2 | 1 |
| AdamW ϵ | $1e - 8$ | |
| AdamW β | (0.9, 0.999) | |
| Peak Learning Rate | $1e - 4$ | |
| Learning Rate Scheduler | ReduceLROnPlateau | N/A |
| Factor & Patience | 0.9, 10 | N/A |
| Dropout | X | |
| Weight Decay | 0.08 | |
| Data Augmentation | Intensity Shift, Rotation, Scaling | |
| Cropped Foreground | ✓ | |
| Intensity Offset | 0.1 | |
| Rotation Degree | -30° to $+30^\circ$ | |
| Scaling Factor | x: 0.1, y: 0.1, z: 0.1 | |

A.2 PUBLIC DATASETS DETAILS

Table 5: Complete Overview of three public MICCAI Challenge Datasets

| MICCAI Challenge | FeTA 2021 | FLARE 2021 | AMOS 2022 |
|-------------------|--|---|---|
| Imaging Modality | 1.5T & 3T MRI | Multi-Contrast CT | Multi-Contrast CT |
| Anatomical Region | Infant Brain | Abdomen | Abdomen |
| Dimensions | $256 \times 256 \times 256$ | $512 \times 512 \times \{37 - 751\}$ | $512 - 768 \times 512 - 768 \times \{68 - 353\}$ |
| Resolution | $\{0.43 - 0.70\} \times \{0.43 - 0.70\} \times \{0.43 - 0.70\}$ | $\{0.61 - 0.98\} \times \{0.61 - 0.98\} \times \{0.50 - 7.50\}$ | $\{0.45 - 1.07\} \times \{0.45 - 1.07\} \times \{1.25 - 5.00\}$ |
| Sample Size | 80 | 361 | 200 |
| Anatomical Label | External Cerebrospinal Fluid (ESF), Grey Matter (GM), White Matter (WM), Ventricles, Cerebellum, Deep Grey Matter (DGM) Brainstem | Spleen, Kidney, Liver, Pancreas | Spleen, Left & Right Kidney, Gall Bladder, Esophagus, Liver, Stomach, Aorta, Inferior Vena Cava (IVC) Pancreas, Left & Right Adrenal Gland (AG), Duodenum, Bladder, Prostates/uterus |